Electron-impact high-lying N_2^- resonant states

He Su ⓘ

College of Physics, Sichuan University, Chengdu, 610065, China
and Department of Physics and Astronomy, University College London, London WC1E 6BT, United Kingdom

Xinlu Cheng ⓘ

Institute of Atomic and Molecular Physics, Sichuan University, Chengdu 610065, China

Bridgette Cooper ⓘ and Jonathan Tennyson ⓘ*

Department of Physics and Astronomy, University College London, London WC1E 6BT, United Kingdom

Hong Zhang ⓘ†

College of Physics, Sichuan University, Chengdu 610065, China

Quasibound states of the nitrogen molecular anion are studied by electron scattering from N_2 using *ab initio* R-matrix theory and a close-coupling model. Scattering calculations are performed using both cc-pVTZ and cc-pVQZ target basis sets involving up to 26 low-lying target states in a complete active space configuration-interaction representation. Complex resonance potential energy curves are characterized as a function of internuclear separation for all eight N_2^- states identified, including the well-known $X\,^2\Pi_g$ shape resonance, one $1\,^2\Sigma_g^+$ Feshbach resonance, as well as six core-excited resonances involving $1\,^2\Delta_g$, $1\,^2\Pi_u$, $2\,^2\Pi_u$, $3\,^2\Pi_u$, $1\,^2\Sigma_u^+$, and $1\,^2\Sigma_u^-$. The $^2\Delta_g$ and $^2\Sigma_u^-$ resonant states are identified and characterized. Comparisons are made with the very different resonance structure in the isoelectronic CO^- anion. The present resonance analysis provides a starting point for studies of the vibrational excitation, electron-impact dissociation, and other resonance-driven phenomena in N_2.

I. INTRODUCTION

The existence of long-lived, quasibound negative-ion states, formed in low-energy electron scattering with molecules, has long been the subject of study [1,2] because of their profound effect on electron collisions. While there are no bound states of the anionic nitrogen molecule (or atom), there has been considerable work on N_2^- resonance states. The energetically lowest state of N_2^- is the $X\,^2\Pi_g$ shape resonance that dominates the electron-N_2 collision cross section between 1.8 and 3.5 eV; the resonance has become a textbook example of shape resonances which has been well studied both theoretically and experimentally for many years [3–11]. As excitation of N_2^- by low-energy electrons is mainly due to resonant scattering processes [12], study of the N_2^- resonance is important for the understanding of nitrogen discharges, plasmas, and surface processes. A recent compilation of electron-N_2 cross sections has been provided by Song *et al.* [13].

While the $X\,^2\Pi_g$ shape resonance gives the most pronounced effect on the overall electron-N_2 cross section, there is evidence, largely experimental, that there are a number of other N_2^- resonance states. Considering these high-lying

resonances, a sharp resonance in electron scattering from N_2 was first reported by Heideman *et al.* [14] in an electron transmission experiment; they detected a resonance at 11.48(5) eV and gave an upper limit of 20 meV for its width, Γ. Subsequently, Comer and Read [15] assigned this resonance as a Feshbach resonance with $^2\Sigma_g^+$ symmetry, which they identified at 11.87 eV with width of 0.6 meV; Comer and Read proposed that the most likely parent state is the $E\,^3\Sigma_g^+$. Sanche and Schulz [16] claimed that $^2\Sigma_g^+$ symmetry resonance can be associated with the compound parent states $E\,^3\Sigma_g^+$ and $a''\,^1\Sigma_g^+$, whose potential energy curves resemble closely the one obtained by the results for the $N_2^-\,^2\Sigma_g^+$ negative-ion state. Hoffmann *et al.* [17] combined two different electron scattering measurements with *ab initio* calculations determining the resonance position as 11.497(2) eV and width as 1.3(2) meV; they supported Comer and Read's deduction that the parent state of this Feshbach resonance is $E\,^3\Sigma_g^+$. Kitajima *et al.* [7] also observed this Feshbach resonance at around 11.5 eV but did not discuss possible parent states.

The core-excited resonances of molecular nitrogen are much less well studied than ground-state resonances because they only produce weak structures in the overall scattering cross sections. Several earlier studies on N_2^- states with $^2\Pi_u$ and $^2\Sigma_u^+$ have been undertaken. Mazeau *et al.* [12] reported observations of $N_2^-\,^2\Sigma_g^+$ and $^2\Pi_u$ core-excited resonances associated with the Rydberg states. Subsequently Čadež [18]

*j.tennyson@ucl.ac.uk
†hongzhang@scu.edu.cn

used a local complex potential to study the core-excited resonant $^2\Pi_u$ resonance which they associated with the $A\,^3\Sigma_u^+$ parent state. The parent states of $^2\Sigma_g^+$, $^2\Pi_u$, and $^2\Sigma_u^+$ resonances have been separately considered by Poparić *et al.* [19] and Meng *et al.* [20]. We note that work on the much simpler H_2^- resonance system has shown that the designation of parent states is often not unique [21]. In general the higher-lying N_2^- resonance states remain poorly characterized.

This situation contrasts rather sharply with that of carbon monoxide, CO, which is isoelectronic with N_2 and has a similar low-lying $^2\Pi$ shape resonance. However, experiments have shown that CO also has a number of, perhaps as many as eight [22], narrow Feshbach resonances at energies ranging from 10 to 14 eV. These resonances have been extensively studied experimentally using both collision studies [1,23–30] and studies of dissociative electron attachment (DEA) [31–34]. One reason why the higher resonances in N_2 are less well studied than those in CO is that both C and O support stable anion states while N does not. This means that DEA, which necessarily occurs via a resonance, can be used as a sensitive monitor of resonance trapping of the electron for CO but not for N_2 molecules. In a recent series of *R*-matrix calculations, Dora and Tennyson [22,35,36] showed that these high-lying CO resonances are indeed narrow and Feshbach in character, and that they can be associated with particular "parent" excited states of CO. Comparisons between these calculations and recent measurements of Zawadzki *et al.* [37,38] show that, at least for excitation to the lower electronic states, they also provided reliable electron-impact electronic excitation cross sections.

There are very few theoretical studies of high-lying nitrogen resonances. In a recent paper we studied electron-impact excitation of N_2 using the *R*-matrix method [11] with a particular emphasis on the excitation processes from the two low-lying metastable electronically excited states of N_2 ($A\,^3\Sigma_u^+$ and $a\,^1\Pi_g$). The calculations were shown to give reliable predictions of the electron-impact excitation cross sections [13]. In this work we extend these calculations, using both larger target basis sets and more excited states in the close-coupling expansion, to study resonances of N_2 in the 10–15 eV region as a function of bond length. As shown below, we identify a complicated sequence of resonances which are qualitatively different from those found in the CO^- system. To the best of our knowledge, there exist no previous *ab initio* theoretical or experimental study which has identified the $^2\Delta_g$ and $^2\Sigma_u^-$ resonance states which appear as sequence core-excited resonances in our calculations. Please check online for all color figures in this work.

II. *R*-MATRIX THEORY

The implementation of electron-molecule scattering calculations using the *ab initio R*-matrix method has been reviewed by one of us [39]. Here we give a brief description highlighting the parts relevant to this calculation. In the *R*-matrix method, the target plus scattering electron $(N+1)$ configuration space is divided into an inner and an outer region by a sphere of radius a, centered on the molecular center of mass. This sphere encloses the *N*-electron target of N_2 and an outer region exterior to this sphere, as shown in Fig. 1. Within
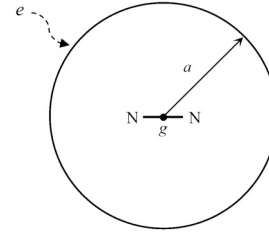

FIG. 1. The *R*-matrix theory divides the space of electron scattering on the N_2 molecule into an inner region and an outer region, and the boundary is given by a sphere of radius $a = 10a_0$ centered on the target center of mass, given by g.

this sphere, the *R*-matrix calculation constructs and solves an energy-independent wave equation giving inner-region wavefunctions of the $(N+1)$-electron scattering system. In this region, the scattering electron interacts strongly with the target electrons through exchange and correlation effects, and as such is accurately modeled using a configuration-interaction basis expansion for the total wavefunction in this region. For the present work, this problem is built by using the complete active space (CAS) configuration interaction (CI) representation of the target wavefunction for which a particularly efficient purpose-built algorithm is used [40]. In the outer region, the scattering electron is only influenced by the dipole and quadrupole moments of the target. The energy-dependent scattering problem is solved by constructing R matrices at a which are then propagated to asymptotic distances and matched with asymptotic solutions yielding K matrices which contain all the required information on the scattering process.

In the inner region, scattering calculations start by constructing an *N*-electron target wavefunction. Then the $(N+1)$ system gives a full description of the target interacting with the scattering electron within the *R*-matrix sphere. The wavefunction for the $(N+1)$-electron system is represented by a close-coupling expansion [39]:

$$\Psi_k^{N+1}(x_1, \ldots, x_{N+1}) = A \sum_{ij} a_{ijk} \varphi_i^N(x_1, \ldots, x_N) u_{ij}(x_{N+1})$$
$$+ \sum_i b_{ik} \chi_i^{N+1}(x_1, \ldots, x_{N+1}), \quad (1)$$

where A is the antisymmetrization operator which accounts for the exchange between the target electrons and the scattering electron, φ_i^N is the wavefunction of the *i*th target state, and χ_i^{N+1}, called L^2 configurations, are obtained by putting $(N+1)$ electrons in target molecular orbitals, which are used to represent the short-range polarization and to relax the orthogonality with the continuum functions. These L^2 configurations comprise three configuration classes: $(\text{core})^4(\text{valence})^{10}(\text{continuum})^1$, $(\text{core})^4(\text{valence})^{11}$, and $(\text{core})^4(\text{valence})^{10}(\text{virtual})^1$. u_{ij} represent the continuum orbitals of the scattering electron, which are labeled by the target state index i as they depend on the symmetry of the particular target state, since the two couple to give the correct overall spatial and spin symmetry of the total wavefunction Ψ_k^{N+1}. Both a_{ijk} and b_{ik} variational parameters are determined by matrix diagonalization of the scattering Hamiltonian; the

a_{ijk} coefficients and the associated energy, E_k, are used to evaluate the R matrix at the sphere boundary, a.

Using the above procedure one can construct a range of different models which depend on the choice of target model and representation of the scattering through Eq. (1). The close-coupling (CC) model used here allows the inclusion of electronically excited target states and therefore is especially suitable for representing Feshbach resonances. The CC scattering model includes a number of low-lying target states, depending upon the target model, which are represented by a CI expansion.

III. CALCULATION DETAILS

A. Target calculations

The N$_2$ CAS CI calculations froze four core electrons and the remaining ten electrons moved freely in a state-averaged CAS defined as $(1\sigma_g, 1\sigma_u)^4(2\sigma_g, 2\sigma_u, 1\pi_u, 3\sigma_g, 1\pi_g, 3\sigma_u)^{10}$. The calculations reported here are performed using the Quantemol Electron Collision (QEC) code [41] which runs both the MOLPRO electronic structure program [42] and the recently published version of UK molecular R-matrix code, UKRMOL+ [43]. In our calculations both codes used Gaussian-type orbitals (GTOs) to represent both the target electrons and the scattering electron. The N$_2$ molecule belongs to the $D_{\infty h}$ point group while we use the D_{2h} point group to solve the scattering problem since MOLPRO, UKRMOL+, and hence QEC only allow Abelian point-group symmetries. Sets of target molecular orbitals in the form of both occupied and virtual orbitals were obtained with cc-pVTZ and cc-pVQZ GTO basis sets; the $X\,^1\Sigma_g^+$, $a'\,^1\Sigma_u^-$, $w\,^1\Delta_u$, and $1\,^1\Sigma_u^+$ states were considered in the state-averaged complete active space self-consistent field (CASSCF) calculations.

After testing a number of target representations and scattering models for N$_2$ high-lying excited states using state-averaged CASSCF with cc-pVTZ and cc-pVQZ basis sets, a total of 41 lowest-lying states are considered for the close-coupling expansion in D_{2h} symmetry which is sufficient to include the $E\,^3\Sigma_g^+$ target state in the cc-pVQZ calculation. There are respectively 25 and 26 target states in $D_{\infty h}$ symmetry based on cc-pVTZ and cc-pVQZ basis sets because of the degenerate states of Π and Δ states; these states are listed in Table I. The potential energy curves (PECs) of the above target states are not continuous at some points if target energies are computed point by point using the underlying MOLPRO program run from the QEC code. However, using MOLPRO directly allows calculations to be started with the wavefunctions from neighboring points which leads to smoother curves [44]. Thus, the present PECs in Figs. 3 and 4 were obtained independently from using the same CASSCF directly from MOLPRO using a grid of 0.01 Å in the range $0.804 \leqslant R \leqslant 1.404$ Å, where R is the internuclear distance between two nitrogen atoms. The equilibrium geometry is $R_e = 1.114$ Å based on cc-pVQZ calculations. Compared with two rounds of cc-pVTZ calculations, the average difference value of PECs for all 25 target states is 0.12 eV. For the cc-pVQZ calculations, there exist two jumps affecting all 26 low-lying target curves located at 1.024 Å and 1.134 Å when using MOLPRO via QEC, and the average differences in value of the PECs are 0.81 eV

TABLE I. The calculated vertical excitation energies in eV from the N$_2$ $X\,^1\Sigma_g^+$ ground state to the respective 24 and 25 lowest-lying states with cc-pVTZ and cc-pVQZ bases at equilibrium bond length, $R_e = 1.114$ Å.

State	cc-pVTZ	cc-pVQZ	Expt. [45]
$A\,^3\Sigma_u^+$	7.55	7.36	7.75
$B\,^3\Pi_g$	8.53	8.12	8.04
$W\,^3\Delta_u$	8.97	8.76	8.88
$B'\,^3\Sigma_u^-$	9.64	9.48	9.67
$a\,^1\Pi_g$	9.87	9.57	9.31
$a'\,^1\Sigma_u^-$	10.21	10.07	9.92
$w\,^1\Delta_u$	10.50	10.40	10.27
$C\,^3\Pi_u$	11.81	11.75	11.19
$1\,^1\Pi_u$	14.23	14.00	
$2\,^3\Sigma_u^+$		15.90	
$1\,^1\Sigma_u^+$	17.07	16.36	
$2\,^3\Pi_u$	17.00	16.57	
$1\,^3\Delta_g$	17.41	16.80	
$2\,^1\Sigma_g^+$	17.34	16.82	
$1\,^3\Sigma_g^-$	18.05	17.27	
$3\,^3\Pi_u$	18.19	17.66	
$2\,^3\Pi_g$	20.55	17.69	
$2\,^1\Pi_g$		17.94	
$2\,^3\Sigma_g^-$	18.53	17.99	
$4\,^3\Pi_u$	18.45	18.22	
$1\,^1\Delta_g$		18.31	
$5\,^3\Pi_u$	19.20	18.73	
$3\,^1\Sigma_g^+$	19.69	18.90	
$2\,^1\Delta_g$	19.08	18.95	
$E\,^3\Sigma_g^+$		19.28	
$2\,^1\Pi_u$	19.46		
$3\,^1\Delta_g$	19.62		
$3\,^1\Pi_u$	19.79		

except for the range 1.024–1.124 Å and 0.77 eV in the range 1.024–1.124 Å.

Table I compares the calculated excitation energies from the $X\,^1\Sigma_g^+$ electronic ground state to 24 and 25 low-lying target states using cc-pVTZ and cc-pVQZ basis sets at the equilibrium structure; the target states obtained here are used in the close-coupling expansion of the scattering wavefunctions in the R-matrix calculations. Compared to the lowest target states obtained from the cc-pVQZ basis set, the $2\,^1\Pi_u$, $3\,^1\Delta_g$, and $3\,^1\Pi_u$ symmetries are generated from cc-pVTZ instead of $2\,^3\Sigma_u^+$, $2\,^1\Pi_g$, $1\,^1\Delta_g$, and $E\,^3\Sigma_g^+$ target states. The excitation energies calculated at the cc-pVTZ level are slightly higher than those of cc-pVQZ, which are closer to the experimental results [45] for each target state, suggesting that the higher-level calculations are more reliable.

B. Scattering calculations

The *ab initio* R-matrix scattering calculations start from the target molecular orbitals. The scattering electron is represented by continuum orbitals which take the form of bond-centered GTOs fitted to Bessel functions with $l \leqslant 4$ [46]. The radius of the R-matrix sphere a was chosen to be $10a_0$. Compared to our previous study [11] we tested the effect of both increasing the target basis set size (calculations with

TABLE II. N_2^- resonance positions (E_r) and widths (Γ) in eV at the N_2 equilibrium structure, $R_e = 1.114$ Å.

Symmetry	cc-pVTZ		cc-pVQZ	
	E_r	Γ	E_r	Γ
$X\,^2\Pi_g$	2.672	0.581	2.503	0.510
$1\,^2\Sigma_g^+$			10.930	5.6×10^{-5}
$1\,^2\Delta_g$	12.037	1.342	11.366	1.068
$1\,^2\Pi_u$	10.882	1.329	9.430	1.115
$2\,^2\Pi_u$			11.541	1.142
$3\,^2\Pi_u$	12.359	1.680	12.270	1.175

both cc-pVTZ and cc-pVQZ basis sets are reported below) and increasing the size of the CC expansion. Only results with the largest 41-state CC expansion considered are given below since this expansion was necessary to include the $E\,^3\Sigma_g^+$ state which Comer and Read [15] suggested was the parent of the $^2\Sigma_g^+$ resonance. Resonances were characterized by a Breit-Wigner profile fit to the eigenphase sums to obtain resonance positions and widths using the program RESON [47].

In addition, the potential energy curves for the N_2 ground $X\,^1\Sigma_g^+$ target state and the hypothetical N_2^- $X\,^2\Pi_g$ bound state for an internuclear distance of 0.704–3.994 Å were computed using the multireference configuration-interaction (MRCI) method with an aug-cc-pVQZ basis set, which is based on the above CASSCF method, and the core and occupied orbitals are same as the above CAS CI calculations, using the MOLPRO program suite. The Supplemental Material [48] provides more details on the two sets of target PECs and resonances curves.

IV. RESULTS AND DISCUSSION

A. N_2^- resonances

Besides the well-known low-lying $X\,^2\Pi_g$ shape resonance, our calculations also identified broad core-excited resonances of $^2\Delta_g$, $^2\Sigma_u^+$, and $^2\Sigma_u^-$ symmetry as well three of $^2\Pi_u$ symmetry. In addition the higher-level cc-pVQZ calculations also found a narrow $1\,^2\Sigma_g^+$ Feshbach resonance.

Table II gives a summary of these resonances for the N_2 equilibrium bond length, $R_e = 1.114$ Å. It shows that the larger cc-pVQZ calculation gives slightly lower resonance energies and narrower widths—improvements one might expect from a variational calculation with larger basis set giving the lower target energies. The difference in the parameters between the two models gives a rough estimate of the uncertainty in their determination. For the $X\,^2\Pi_g$ resonance, the cc-pVQZ basis set places the resonance at 2.503 eV with a width of 0.510 eV, which is in good agreement with the semiempirical resonance position of 2.34 eV and width of 0.449 eV derived by Laporta et al. [10] as part of their model, which gives excellent agreement with the observed resonance-driven vibrational excitation cross sections [13].

The $1\,^2\Sigma_g^+$ resonant state at 10.930 eV has a narrow width of 0.056 meV in our calculations; this can therefore be identified as a Feshbach resonance. It lies somewhat lower than the experimentally determined position and width: 11.48(5) eV
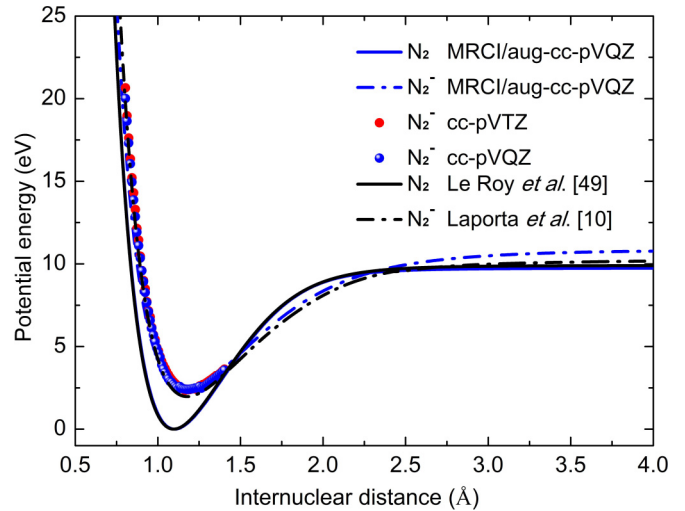

FIG. 2. Comparison of ground N_2 $X\,^1\Sigma_g^+$ target state (black solid line) and N_2^- $X\,^2\Pi_g$ bound state (blue dash-dotted line) PECs, with the resonant $X\,^2\Pi_g$ curves (red and blue dots) with the reference semiempirical curves of Le Roy et al. [49] (black solid line) and Laporta et al. [10] (black dash-dotted line).

and an upper limit of 20 meV by Heideman et al. [14], 11.345 eV and 0.6 meV by Comer and Read [15], the 11.497(2) eV and 1.3(2) meV by Hoffmann et al. [17], and 11.497 eV and 1.42(26) meV by Kitajima et al. [7]. Next we consider how this and the other resonances behave as a function of N_2 internuclear separation, R.

The new core-excited $1\,^2\Delta_g$ resonant state arises in our calculations as degenerate resonances of ^2A_g and $^2B_{1g}$ symmetries; these show a significant shift with model being located at 12.037 eV in the cc-pVTZ basis set and 11.366 eV in the cc-pVQZ basis set. There are no previous reports of a $1\,^2\Delta_g$ state. The cc-pVQZ target basis set predicts three $^2\Pi_u$ resonances which are broad with widths 1 eV at R_e; this sort of broad width in the region of excited target states is usually associated with core-excited shape resonance. The lowest $^2\Pi_u$ ($1\,^2\Pi_u$) also shows a pronounced shift in energy with the model. At the equilibrium bond length, the second $2\,^2\Pi_u$ resonance is only detected in the cc-pVQZ calculation. This resonance is detected at longer bond length in the cc-pVTZ calculation (see below). Resonances with $^2\Sigma_u^+$ and $^2\Sigma_u^-$ symmetry, which both also appear to be core-excited shape resonances, are also only detected for $R > R_e$.

To show the full behavior and analyze these various resonances, we determined the resonant state curves as a function of internuclear distance and attempted to identify any corresponding parent states. The present resonant energy curves are calculated by adding the resonance position to the ground target energy from direct MOLPRO at each geometry. Figure 2 shows the calculated N_2 $X\,^1\Sigma_g^+$ and N_2^- $X\,^2\Pi_g$ PECs computed at the MRCI/aug-cc-pVQZ level of theory using MOLPRO. These curves give an excellent agreement with the very accurate, semiempirical curves of Le Roy et al. [49] for N_2 and Laporta et al. [10] for N_2^-. Our calculations respectively give dissociation energies for N_2 and N_2^- of 9.74 and 8.36 eV [assuming that $N^-(^2P)$ lies 0.07 eV above $N(^4S)$
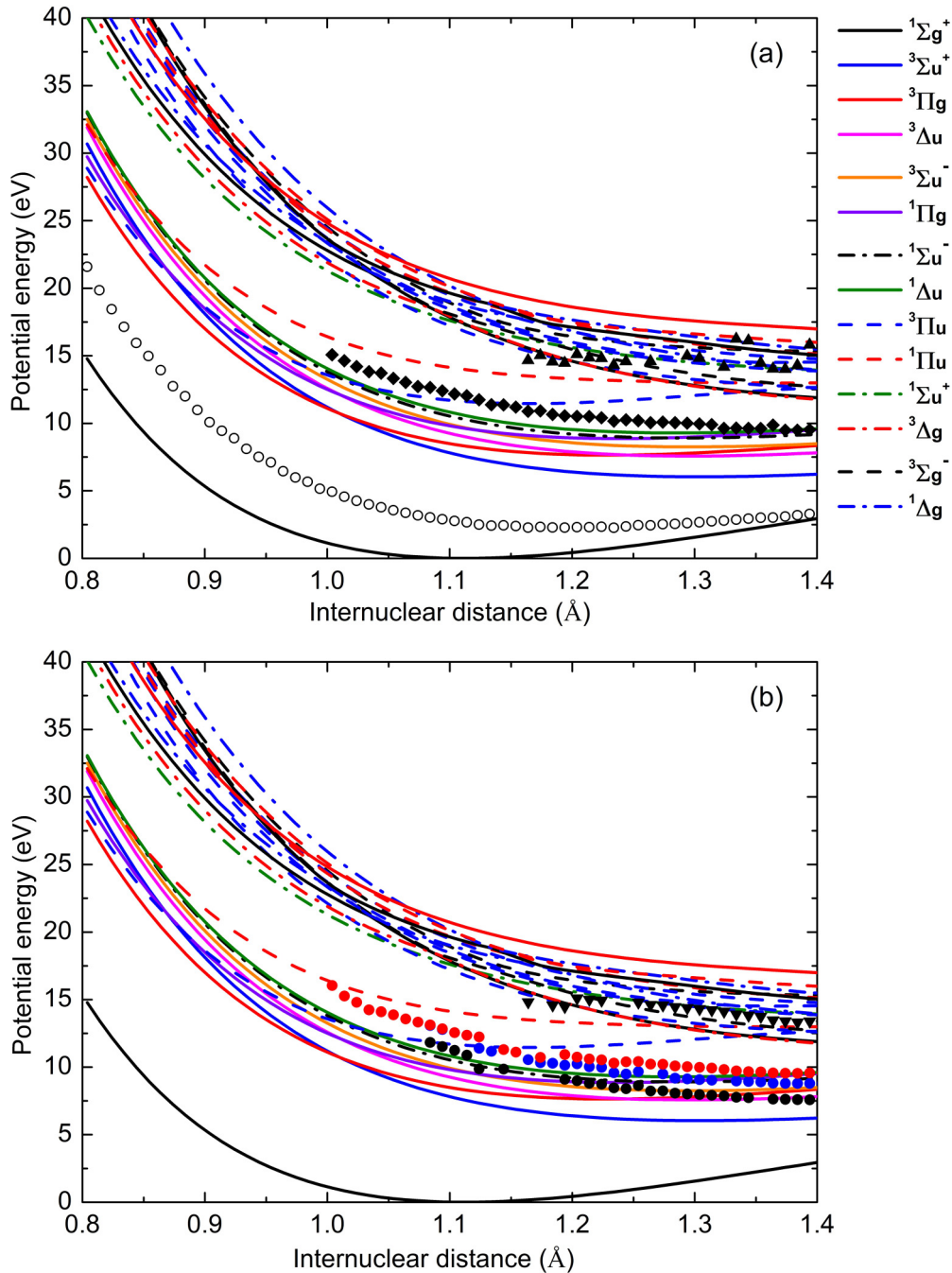
FIG. 3. N$_2$ PECs for 25 lowest-lying electronic states based on cc-pVTZ level, compared to N$_2$$^-$ symmetry resonance curves: (a) ○, X $^2\Pi_g$; ◆, 1 $^2\Delta_g$; ▲, 1 $^2\Sigma_u^+$; (b) ●, 1 $^2\Pi_u$; ●, 2 $^2\Pi_u$; ●, 3 $^2\Pi_u$; ▼, 1 $^2\Sigma_u^-$. All energies are given relative to the minimum of the X $^1\Sigma_g^+$ N$_2$ ground state.

[50]], which can be compared well to 9.765 eV of Hendrie [51] and 8.22 eV of Laporta *et al.* [10]. The X $^2\Pi_g$ shape resonance curves obtained from two models match well with the MOLPRO MRCI/aug-cc-pVQZ N$_2$$^-$ state calculations. The X $^2\Pi_g$ is a bound state only in the intermediate region $1.494 < R < 2.284$ Å. Beyond 2.284 Å, this state becomes a resonance again going asymptotically to N(^4S) plus the anion resonance state N$^-$(^2P).

Figures 3 and 4 present our other N$_2$$^-$ high-lying resonance energy curves; for comparison our calculated N$_2$ target state PECs respectively are also given. As can be seen, our

calculations do not detect resonances for all R. Some resonances, such as the 1 $^2\Sigma_g^+$ Feshbach resonance, are only detected in our Fig. 4(a), and the 2 $^2\Pi_u$ in Fig. 4(b) only occurs for $R \geqslant 1.004$ Å. This is probably due to the limitations of our resonance fitting procedure which does not work for resonances which are located very close to a target state. As shown below, the width of these resonances increases rapidly with decreasing R; that such broad resonances eventually become undetectable at short R is well known from studies of the X $^2\Sigma_u^+$ resonance in H$_2$ [52]. Especially, it is difficult to detect high-lying resonances at intermediate geometries. The

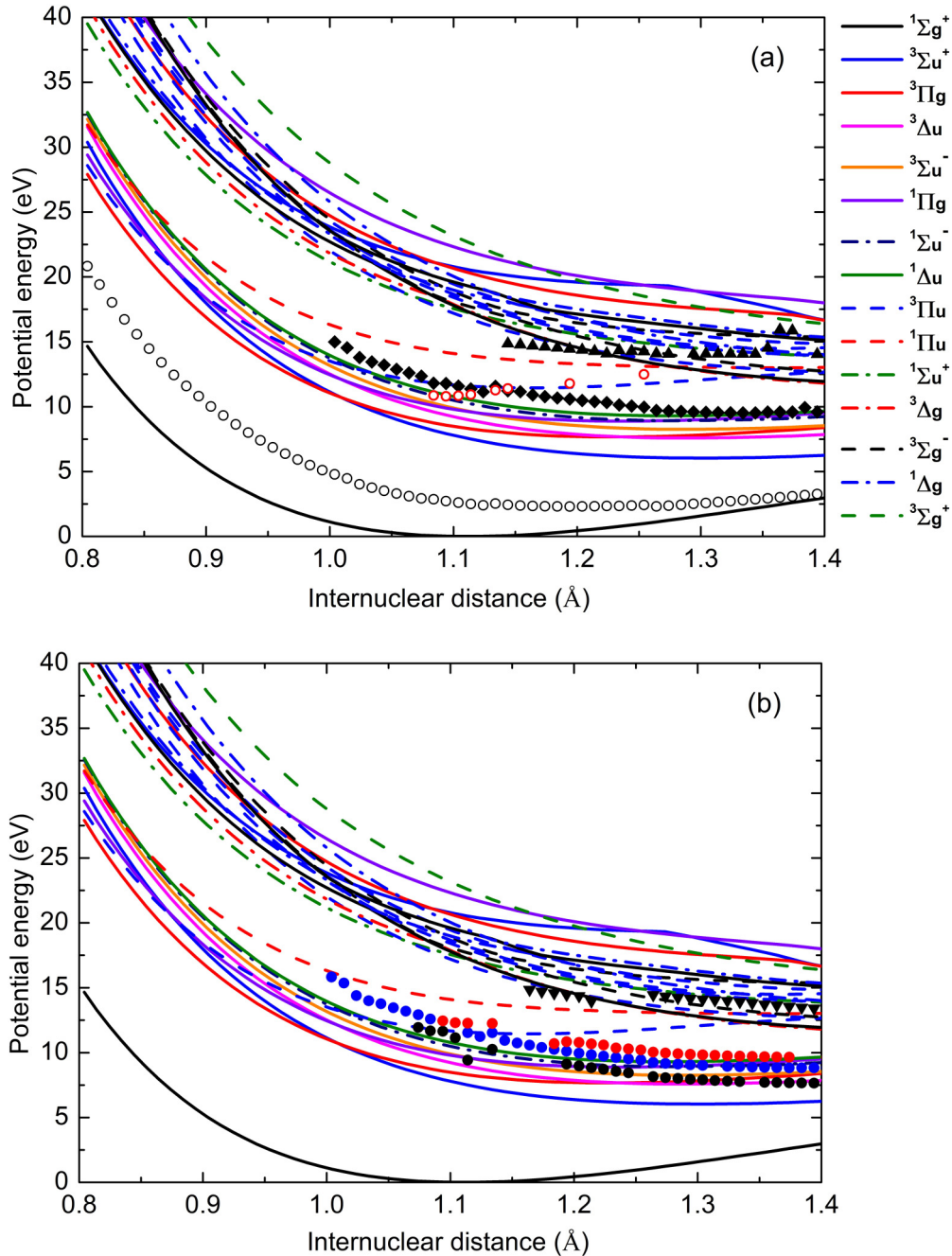FIG. 4. N_2 PECs for 26 lowest-lying electronic states based on cc-pVQZ level, compared to N_2^- symmetry resonance curves: (a) ○, $X\,^2\Pi_g$; ○, $1\,^2\Sigma_g^+$; ◆, $1\,^2\Delta_g$; ▲, $1\,^2\Sigma_u^+$; (b) ●, $1\,^2\Pi_u$; ●, $2\,^2\Pi_u$; ●, $3\,^2\Pi_u$; ▼, $1\,^2\Sigma_u^-$. All energies are given relative to the minimum of the $X\,^1\Sigma_g^+$ N_2 ground state.

$1\,^2\Sigma_g^+$ Feshbach resonance is only detected in our cc-pVQZ calculation in the range $1.084 \leqslant R \leqslant 1.194$ Å. Although our models include target states up to the $E\,^3\Sigma_g^+$ state which might be associated to get the $^2\Sigma_g^+$ resonance, it is hard to unequivocally identify the parent state of the $1\,^2\Sigma_g^+$ resonance. The present calculations suggest that it belongs to neither the $E\,^3\Sigma_g^+$, as assigned by Comer and Read [15], nor the $a\,^1\Pi_g$ and $B\,^3\Pi_g$ states, as suggested by Poparić *et al.* [19] and Meng *et al.* [20]. Indeed our $1\,^2\Sigma_g^+$ resonance curve does not seem to track any of the N_2 target states. The $E\,^3\Sigma_g^+$

state is a Rydberg state; the present computational procedure only approximately characterizes this target PEC with the cc-pVQZ basis set which contains no augmented diffuse basis functions. Use of augmented basis sets leads to the need to use very extended inner regions and leads to considerable computational complications [53]. Thus, there is a need for further analysis on the parent state of the $1\,^2\Sigma_g^+$ Feshbach resonance.

The newly identified core-excited $1\,^2\Delta_g$ resonance nearly overlaps with $1\,^2\Pi_u$ and $2\,^2\Pi_u$ resonant curves (see Figs. 3 and 4). The $1\,^2\Delta_g$ resonance energy curve is close to the $w\,^1\Delta_u$
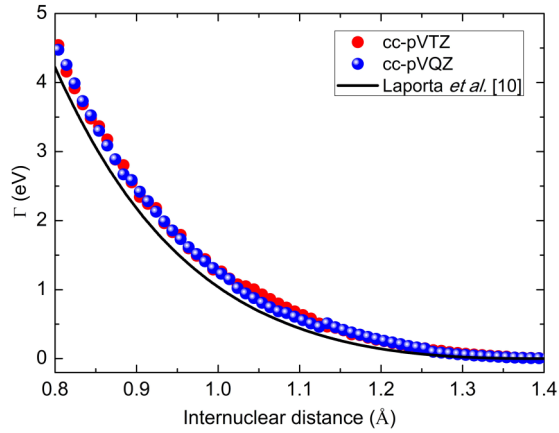
FIG. 5. N$_2^-$ $X\,^2\Pi_g$ resonance widths (Γ) as a function of internuclear distance compared to Laporta *et al.* [10].

FIG. 6. N$_2^-$ $1\,^2\Sigma_g^+$ resonance widths (Γ) as a function of internuclear distance.

(green solid line) and $a'\,^1\Sigma_u^-$ (black dash-dotted line) PECs which can be identified in Figs. 3(a) and 4(a) associated with an order of target states listed in Table I, which are therefore reasonably assumed to be its parent states. The three $^2\Pi_u$ resonances appear to swap parent states as a function of the internuclear separation, as likewise discussed in the parent state swapping behavior of H$_2^-$ [21] and CO$^-$ resonances [22]. Thus, we cannot confirm the $A\,^3\Sigma_u^+$ parent state assignment of Čadež [18]. The $1\,^2\Sigma_u^+$ and $1\,^2\Sigma_u^-$ symmetries are responsible for core-excited resonances as shown in Figs. 4(a) and 4(b). Both resonant positions appear to be only weakly dependent on R and not to correlate with any particular set of target states; these two resonance energies are higher than 10 eV for all Rs for which they are detected.

The corresponding resonance widths Γ as a function of internuclear distance are given in Figs. 5–9. These resonance widths generally drop towards zero at large R. Any discontinuity in the resonance energy also affects the resonance width. In general the widths are more sensitive to the level of theory used and the fit parameters so show more scatter than the PECs. Furthermore, if a resonance crosses a target state then the resonance width usually changes significantly [54], but the resonance energy curve remains smooth. In addition the underlying MOLPRO target curves are not always smooth due to the need to compute each point independently in the QEC code, and such changes usually manifest themselves in the widths. Figure 5 shows that our $X\,^2\Pi_g$ resonance width curves agree well with that assumed by Laporta *et al.* [10] but not the earlier study by the same authors [9] which assumed that the resonance got narrower at small R.

Our cc-pVQZ calculations show two small jumps at around 1.024 and 1.134 Å which are associated with the discontinuities in the underlying target electronic structure calculations at these geometries, which is caused by orbital swaps in the target CAS. Actually, the resonance positions show little sensitivity to the target state discontinuities. This jump is small and only weakly impacts our predicted positions and widths. However, the resonance widths for both basis sets nearly overlap except for the range $1.024 \leqslant R \leqslant 1.124$ Å.

The $1\,^2\Sigma_g^+$ Feshbach resonance is very narrow (see Fig. 6), in line with the observations in Refs. [15–17,55], and our
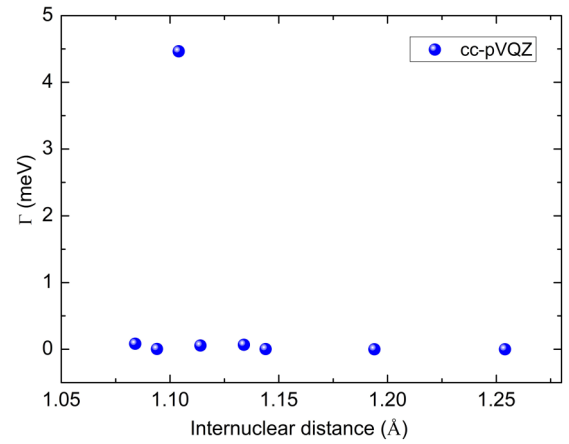
$\Gamma(R)$ is less than 0.1 meV except at $R = 1.104$ where the fit gives $\Gamma = 4.464$ meV; tests show that this increased width is robust and not just due artifacts of the calculation. We note that this geometry is the first at which the $1\,^2\Sigma_g^+$ resonance curve moves above the $w\,^1\Delta_u$ [green solid line in Fig. 4(a)] target state. As R further increases, the resonance becomes increasingly narrow with Γ only 2.8×10^{-6} meV at $R = 1.254$ Å, the last geometry for which we were able to detect it. In Fig. 7, it seems that the two basis set calculations give similar results for the $1\,^2\Delta_g$ resonance. Figure 8 shows that the three $1\,^2\Pi_u$, $2\,^2\Pi_u$, and $3\,^2\Pi_u$ resonance width curves become smoother as R increases; fits to narrower resonances are inherently more stable and more reliable. Finally, Fig. 9 shows that the $1\,^2\Sigma_u^+$ and $1\,^2\Sigma_u^-$ resonance widths generally decrease systematically with increasing R.

B. Comparisons with CO$^-$

One would expect electron scattering from the N$_2$ molecule would have similarities with electron scattering from CO, as both have 14 electrons. We therefore provide a comparison of
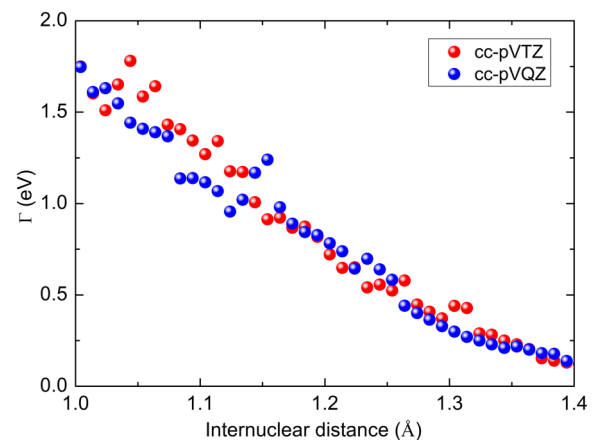

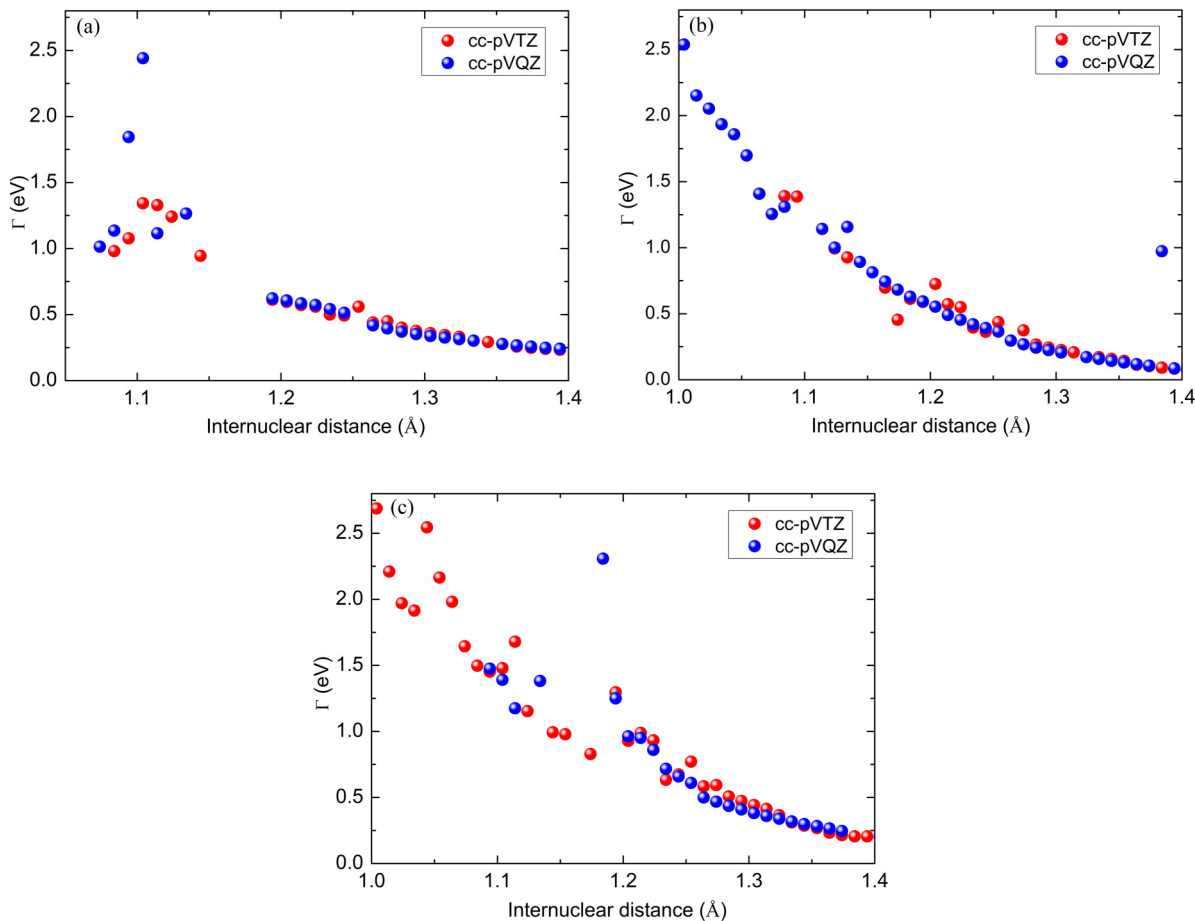FIG. 7. N$_2^-$ $1\,^2\Delta_g$ resonance widths (Γ) as a function of internuclear distance.

FIG. 8. N_2^- (a) $1\,^2\Pi_u$, (b) $2\,^2\Pi_u$, and (c) $3\,^2\Pi_u$ resonance widths (Γ) as a function of internuclear distance.

N_2^- and CO^- resonant states based on the recent R-matrix study of CO^- resonances by Dora and Tennyson [22].

Both systems have a well-known, broad, and low-lying (about 2 eV) $^2\Pi$ shape resonance. Dora and Tennyson found eight higher-lying CO^- resonant states involving three of $^2\Sigma^+$ symmetry, four of $^2\Pi_u$, and one $^2\Delta$. All these resonances are narrow with widths of under 0.2 eV for all R and can clearly be identified as Feshbach in nature. For N_2^-, we find seven resonances in the same energy region, but only one, with $^2\Sigma_g^+$

symmetry, can clearly be identified as a Feshbach resonance. The other six resonances, one of $^2\Delta_g$ symmetry, three of $^2\Pi_u$, one of $^2\Sigma_u^+$, and one of $^2\Sigma_u^-$, are all broad with widths of over 1 eV at shorter bond lengths. These resonances all appear to be core-excited shape resonances which means they lie above their parent target state, unlike the classic Feshbach resonance which lies just below its parent, often only just below.

Of course, CO is a polar molecule. While the permanent dipole of the ground state is small and shows a rather compli-
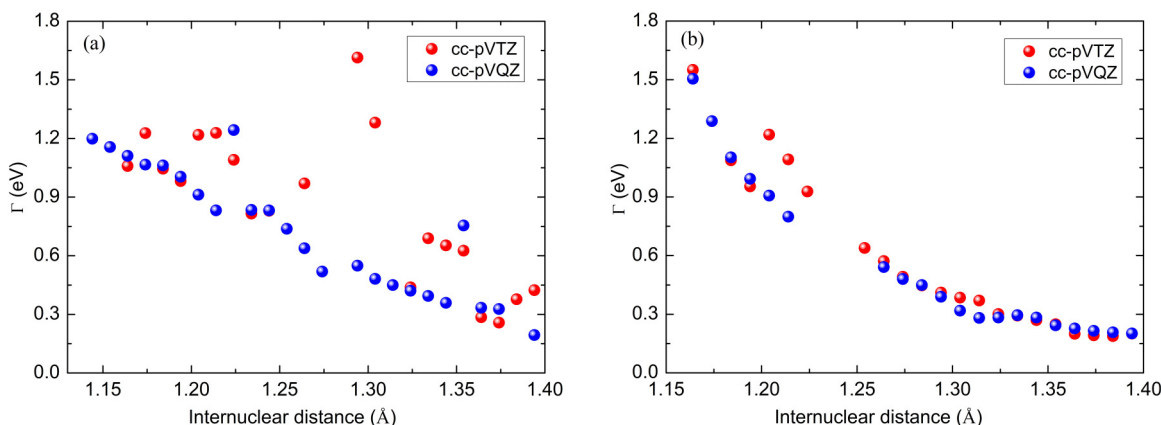

FIG. 9. N_2^- (a) $1\,^2\Sigma_u^+$ and (b) $1\,^2\Sigma_u^-$ resonance widths (Γ) as a function of internuclear distance.

cated behavior with R [56], the permanent dipole moments of the excited target states are larger. This leads to an extra source of binding for the scattering electron. It would appear that the presence of these dipoles results in CO core-excited Feshbach resonances dropping below their target states and becoming Feshbach resonances with the consequent large reduction in resonance width. As noted in the Introduction, fewer N$_2^-$ resonance states have been observed experimentally than for CO$^-$. In particular there are no observations of the newly proposed $^2\Delta_g$ and $^2\Sigma_u^-$ symmetry N$_2$ resonances.

V. CONCLUSIONS

A detailed study of eight quasibound or resonance states of N$_2^-$ are reported using a close-coupling (CC) expansion as part of an *ab initio* R-matrix method. The $^2\Delta_g$ and $^2\Sigma_u^-$ core-excited resonant states are previously undetected. The well-known and well-characterized low-lying $X\,^2\Pi_g$ shape resonance energies match the precisely calculated N$_2^-$ potential curves very well. The higher-level calculations based on the use of a CASSCF cc-pVQZ target representation appear to give a good representation of the N$_2^-$ resonance states, and provide the $^2\Sigma_g^+$ and one more $^2\Pi_u$ resonances at the equilibrium structure. The discontinuities in the resonance width are mainly due to the nature of a given resonance changing as it crosses a target state.

The isoelectronic CO$^-$ appears to comprise of a low-lying $^2\Pi$ shape resonance and then only Feshbach resonances which can be clearly identified with parent states. In contrast, we find only one classic Feshbach resonance of $^2\Sigma_g^+$ symmetry and six broad, core-excited Feshbach resonances. We suggest that this difference could be due to the polar nature of the excited states of the CO target system which leads to extra binding of the scattering electron.

The present work helps to characterize the metastable N$_2^-$ electronic states in the 10–15 eV region which have been little studied up to now. Such resonances especially can strongly affect the vibrational excitation and dissociation of the species in a plasma. Our calculated target and resonant curves will be used to predict high-energy N$_2$ vibrational excitation cross sections in a future study.

[1] G. J. Schulz, Rev. Mod. Phys. **45**, 423 (1973).

[2] H. Hotop, M. W. Ruf, M. Allan, and I. I. Fabrikant, Adv. At. Mol. Phys. **49**, 85 (2003).

[3] T. Rescigno, A. Orel, and C. McCurdy, J. Chem. Phys. **73**, 6347 (1980).

[4] M. Allan, J. Phys. B: At. Mol. Phys. **18**, 4511 (1985).

[5] L. A. Morgan, J. Phys. B: At. Mol. Phys. **19**, L439 (1986).

[6] C. J. Gillan, C. J. Noble, and P. G. Burke, J. Phys. B: At. Mol. Opt. Phys. **21**, L53 (1988).

[7] M. Kitajima, T. Kishino, T. Okumura, N. Kobayashi, A. Sayama, Y. Mori, K. Hosaka, T. Odagiri, M. Hoshino, and H. Tanaka, Eur. Phys. J. D **71**, 139 (2017).

[8] C. J. Gillan, J. Tennyson, B. M. McLaughlin, and P. G. Burke, J. Phys. B: At. Mol. Opt. Phys. **29**, 1531 (1996).

[9] V. Laporta, R. Celiberto, and J. M. Wadehra, Plasma Sources Sci. Technol. **21**, 055018 (2012).

[10] V. Laporta, D. A. Little, R. Celiberto, and J. Tennyson, Plasma Sources Sci. Technol. **23**, 065002 (2014).

[11] H. Su, X. Cheng, H. Zhang, and J. Tennyson, J. Phys. B: At. Mol. Opt. Phys. **54**, 115203 (2021).

[12] J. Mazeau, R. Hall, G. Joyez, M. Landau, and J. Reinhardt, J. Phys. B **6**, 873 (1973).

[13] M.-Y. Song, H. Cho, G. P. Karwasz, V. Kokoouline, and J. Tennyson, J. Phys. Chem. Ref. Data (2022).

[14] H. Heideman, C. Kuyatt, and G. Chamberlain, J. Chem. Phys. **44**, 355 (1966).

[15] J. Comer and F. Read, J. Phys. B **4**, 1055 (1971).

[16] L. Sanche and G. Schulz, Phys. Rev. A **6**, 69 (1972).

[17] T. Hoffmann, M. Allan, K. Franz, M. Ruf, H. Hotop, G. Sauter, and W. Meyer, J. Phys. B: At. Mol. Opt. Phys. **42**, 215202 (2009).

[18] I. Čadež, Planet. Space Sci. **31**, 843 (1983).

[19] G. Poparić, M. Vićić, and D. Belić, Chem. Phys. **240**, 283 (1999).

[20] X. Meng, B. Wu, X.-F. Gao, J.-C. Xie, H. Li, Y. Yu, D.-F. Zhao, and S. X. Tian, J. Chem. Phys. **153**, 024301 (2020).

[21] D. T. Stibbe and J. Tennyson, J. Phys. B: At. Mol. Opt. Phys. **30**, L301 (1997).

[22] A. Dora and J. Tennyson, J. Phys. B: At. Mol. Opt. Phys. **53**, 195202 (2020).

[23] L. Sanche and G. J. Schulz, Phys. Rev. Lett. **26**, 943 (1971).

[24] J. Mazeau, F. Gresteau, G. Joyez, J. Reinhardt, and R. I. Hall, J. Phys. B: At. Mol. Phys. **5**, 1890 (1972).

[25] J. Mazeau, C. Schermann, and G. Joyez, J. Electron Spectrosc. Relat. Phenom. **7**, 269 (1975).

[26] B. Wallbank, S. Daviel, J. Comer, and P. Hickes, J. Phys. B: At. Mol. Phys. **16**, 3065 (1983).

[27] D. S. Newman, M. Zubek, and G. C. King, J. Phys. B: At. Mol. Phys. **16**, 2247 (1983).

[28] J. P. Polley and T. L. Bailey, Phys. Rev. A **37**, 733 (1988).

[29] A. G. Middleton, M. J. Brunger, and P. J. O. Teubner, J. Phys. B: At. Mol. Opt. Phys. **26**, 1743 (1993).

[30] R. Olszewski, P. Woliski, and M. Zubek, Chem. Phys. Lett. **297**, 537 (1998).

[31] P. Nag and D. Nandi, Phys. Chem. Chem. Phys. **17**, 7130 (2015).

[32] S. X. Tian, B. Wu, L. Xia, Y.-F. Wang, H.-K. Li, X.-J. Zeng, Y. Luo, and J. Yang, Phys. Rev. A **88**, 012708 (2013).

[33] X.-D. Wang, C.-J. Xuan, Y. Luo, and S. X. Tian, J. Chem. Phys. **143**, 066101 (2015).

[34] K. Gope, V. Tadsare, V. S. Prabhudesai, N. J. Mason, and E. Krishnakumar, Eur. Phys. J. D **70**, 134 (2016).

[35] A. Dora, J. Tennyson, and K. Chakrabarti, Eur. Phys. J. D **70**, 197 (2016).

[36] A. Dora and J. Tennyson, in *Quantum Collisions and Confinement of Atomic and Molecular Species, and Photons*, edited by P. C. Deshmukh, E. Krishnakumar, S. Fritzsche, M. Krishnamurthy, and S. Majumder (Springer, Singapore, 2019), Vol. 230, pp. 48–59.

[37] M. Zawadzki, M. A. Khakoo, L. Voorneman, L. Ratkovic, Z. Mašín, K. Houfek, A. Dora, and J. Tennyson, J. Phys. B: At. Mol. Opt. Phys. **53**, 165201 (2020).

[38] M. Zawadzki, M. A. Khakoo, A. Sakaamini, L. Voorneman, L. Ratkovic, Z. Mašín, A. Dora, R. Laher, and J. Tennyson, J. Phys. B: At. Mol. Opt. Phys. **55**, 025201 (2022).

[39] J. Tennyson, Phys. Rep. **491**, 29 (2010).

[40] J. Tennyson, J. Phys. B: At. Mol. Opt. Phys. **29**, 1817 (1996).

[41] B. Cooper, M. Tudorovskaya, S. Mohr, A. O'Hare, M. Hanicinec, A. Dzarasova, J. Gorfinkiel, J. Benda, Z. Mašín, A. Al-Refaie, P. J. Knowles, and J. Tennyson, Atoms **7**, 97 (2019).

[42] H.-J. Werner, P. J. Knowles, F. R. Manby, J. A. Black, K. Doll, A. Heßelmann, D. Kats, A. Köhn, T. Korona, D. A. Kreplin *et al.*, J. Chem. Phys. **152**, 144107 (2020).

[43] Z. Mašín, J. Benda, J. D. Gorfinkiel, A. G. Harvey, and J. Tennyson, Comput. Phys. Commun. **249**, 107092 (2020).

[44] A. T. Patrascu, C. Hill, J. Tennyson, and S. N. Yurchenko, J. Chem. Phys. **141**, 144312 (2014).

[45] J. Oddershede, N. E. Grüner, and G. H. Diercksen, Chem. Phys. **97**, 303 (1985).

[46] A. Faure, J. D. Gorfinkiel, L. A. Morgan, and J. Tennyson, Comput. Phys. Commun. **144**, 224 (2002).

[47] J. Tennyson and C. J. Noble, Comput. Phys. Commun. **33**, 421 (1984).

[48] See Supplemental Material at http://link.aps.org/supplemental/10.1103/PhysRevA.105.062824 for N_2 target potential energy curves and N_2^- resonance parameters as a function of internuclear distance obtained from cc-pVTZ and cc-pVQZ basis sets.

[49] R. J. Le Roy, Y. Huang, and C. Jary, J. Chem. Phys. **125**, 164310 (2006).

[50] J. Mazeau, F. Gresteau, R. Hall, and A. Huetz, J. Phys. B: At. Mol. Phys. **11**, L557 (1978).

[51] J. Hendrie, J. Chem. Phys. **22**, 1503 (1954).

[52] D. T. Stibbe and J. Tennyson, J. Phys. B: At. Mol. Opt. Phys. **31**, 815 (1998).

[53] T. Meltzer and J. Tennyson, J. Phys. B: At. Mol. Opt. Phys. **53**, 245203 (2020).

[54] D. A. Little and J. Tennyson, J. Phys. B: At. Mol. Opt. Phys. **47**, 105204 (2014).

[55] D. S. Slaughter, D. J. Haxton, H. Adaniya, T. Weber, T. N. Rescigno, C. W. McCurdy, and A. Belkacem, Phys. Rev. A **87**, 052711 (2013).

[56] V. V. Meshkov, A. Y. Ermilov, A. V. Stolyarov, E. S. Medvedev, V. G. Ushakov, and I. E. Gordon, J. Quant. Spectrosc. Radiat. Transfer **280**, 108090 (2022).